Supplementary Material: Disconnecting a Traversable Wormhole: Universal Quench Dynamics in Random Spin Models

Tian-Gang Zhou,[1] Lei Pan,[1] Yu Chen,[2] Pengfei Zhang,[3,4,*] and Hui Zhai[1,†]

[1] *Institute for Advanced Study, Tsinghua University, Beijing,100084, China*
[2] *Graduate School of China Academy of Engineering Physics, Beijing, 100193, China*
[3] *Institute for Quantum Information and Matter, California Institute of Technology, Pasadena, California 91125, USA*
[4] *Walter Burke Institute for Theoretical Physics, California Institute of Technology, Pasadena, California 91125, USA*

(Dated: December 1, 2020)

I. EXACT DIAGONALIZATION

Here we report the results from the exact diagonalization calculation of a finite-size spin system, which shows both the slow dynamics and the oscillatory dynamics in different parameter regimes. The results are consistent with those reported in the main text based on the large-N expansion and assuming the melon diagrams. This consistency provides supports to our approximations used in the main text. Nevertheless, we should also emphasize that, because the finite-size exact diagonalization and large-N theory are two different approximations, we do not expect a quantitative agreement between these two calculations.

Firstly, slow dynamics is shown in the Fig. 1(A) and (B). In the same parameter region as in our large-N theory discussed in the main text, we observe the stretched exponential decay behavior of M^x. In the $\log(|\log M^x|) - \log t$ coordinates, we find the decay exponent $\eta < 1$.

Secondly, we find some hints for the oscillatory behavior as shown in Fig. 1(C). Here we should first note that the symmetry breaking behaviors can hardly be achieved in such a small size spin system with $N = 10$ by the exact diagonalization method. In fact, we do not find oscillatory behavior in the exact diagonalization calculation when we quench the external field h to zero. This is actually consistent with our conclusion that the oscillatory behavior is associated with the final state in the TW phase, where M^x is non-zero. Hence, to show the oscillatory behavior in the exact diagonalization calculations, we quench h to a very small value, say, $h = 0.02$, instead of $h = 0$. The results are shown in Fig. 1(C). It shows that for small βJ, at a long time the magnetization saturates to a constant, with very small variation. As βJ increases, the long time dynamics exhibits a larger and larger variation around its long-time averaged value, although the variation is not a perfect oscillation due to the finite-size effect.

II. LOW-ENERGY EFFECTIVE ACTION

A. Equilibrium Solution

Here we will discuss the low-energy effective action for the random spin model in the TW phase. We can identify two parts of contributions in addition to the Schwarzian action. The first part corresponds to the transverse magnetic field $h_{\rm tol}$, the effect of which has already been considered in the Maldacena-Qi's work [1]. The second part represents the effect from a non-zero Δ, with the assumption that $|\Delta| \ll 1$. Here we show how these two quantities affect the energy gap $E_{\rm gap}$ in the TW phase, and the equilibrium magnetization M^x.

To begin with, it is known that under the melon-diagram approximation, the effective action in the imaginary time can be written as

$$\begin{aligned}\frac{\mathcal{I}}{N} = &- \operatorname{Tr}\log(\partial_\tau - \Sigma) - \int \mathrm{d}\tau_1\,\mathrm{d}\tau_2 \left[\operatorname{Tr}\left[\Sigma(\tau_1,\tau_2)G(\tau_2,\tau_1)\right] + \sum_{\alpha\alpha'} \frac{J^2}{16}\xi^\alpha\xi^{\alpha'} \left(\operatorname{Tr}\left[\sigma^\alpha G(\tau_1,\tau_2)\sigma^{\alpha'}G(\tau_2,\tau_1)\right]\right)^2 \right] \\ &+ \int \mathrm{d}\tau_1 \frac{h_{\rm tol}}{2}\operatorname{Tr}\left[G(\tau_1,\tau_1)\sigma_x\right].\end{aligned} \tag{1}$$

* pengfeizhang.physics@gmail.com
† hzhai@tsinghua.edu.cn

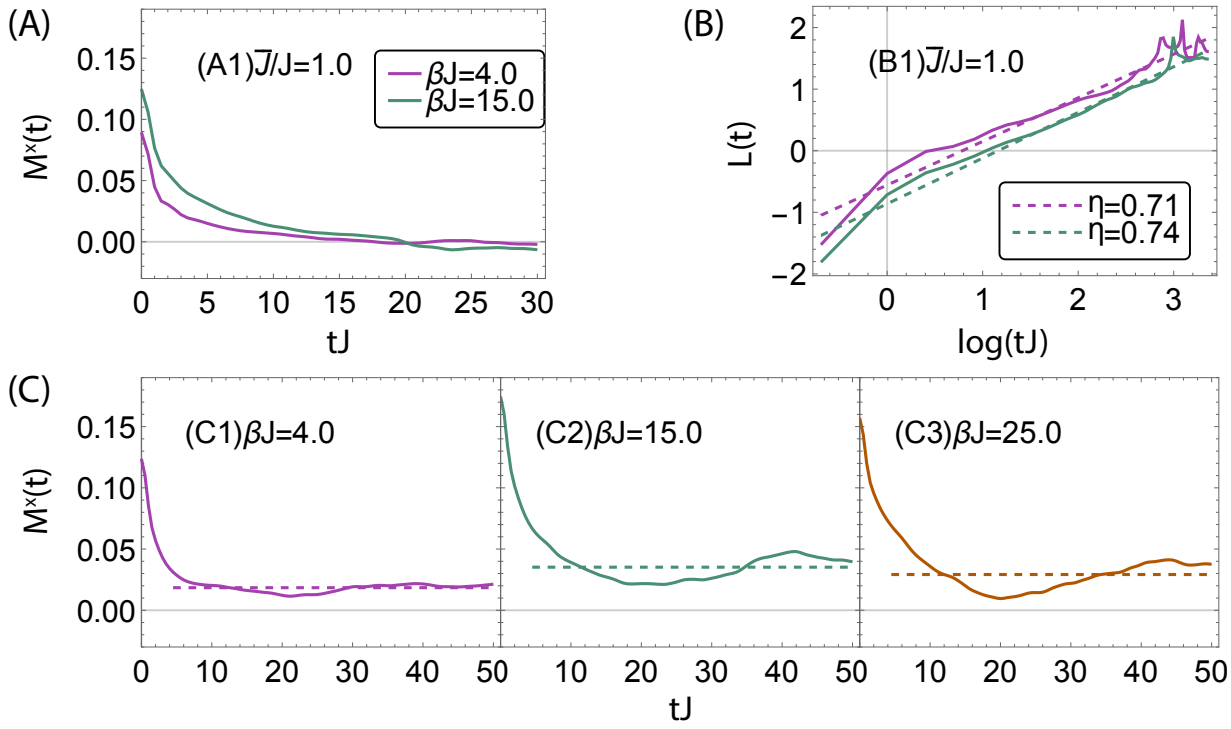

FIG. 1. **Result of Exact Diagonalization.** The results from the exact diagnolization calculation of the random spin model Eq. (1) in the main text, with the number of spins $N = 10$. The quench dynamics is averaged over 60 different disorder configurations. (A) Quench dynamics in $\bar{J} = 0$ and $\Delta = -0.73$, corresponding to the Fig. 3 in the main text. Initially, the system is prepared at $h = 0.2J$, and we completely turn off h to observe the stretched exponential decay. (B) The same data but in the $\log(|\log M^x|) - \log t$ coordinates. Here we show the decay exponent η in the figure. (C) Quench dynamics in $\bar{J} = 0$ and $\Delta = -0.5$, corresponding to the Fig. 4 in the main text. Initially system is prepared at $h = 0.2J$. For (A) and (B), h is quenched to zero, but for (C), h is quenched to $0.02J$. The dashed line in (C) is the long-time averaged value.

Here we define the imaginary-time Green's function as:

$$G_{ss'}(\tau) = \frac{1}{N}\sum_i \left\langle \mathcal{T}_\tau \hat{c}_{i,s}(\tau)\hat{c}^\dagger_{i,s'}(0)\right\rangle. \tag{2}$$

Here $s, s' = \uparrow$ or $\downarrow$ are the up or down spin indices respectively. From now on, we focus on the small $h_{\rm tol}/J$, where the dynamics can be described by the evolution of reparametrization modes. After imposing the spin rotational symmetries and the particle-hole symmetries discussed in the main text, direct calculation shows

$$\begin{aligned}&\sum_{\alpha\alpha'}\frac{J^2}{16}\xi^\alpha\xi^{\alpha'}\left(\mathrm{Tr}\left[\sigma^\alpha G(\tau_1,\tau_2)\sigma^{\alpha'}G(\tau_2,\tau_1)\right]\right)^2\\ =&\frac{J^2}{4}\Big[\left(\Delta^2+2\right)G_{\uparrow\uparrow}(\tau_1,\tau_2)^4+\left(\Delta^2+2\right)G_{\uparrow\downarrow}(\tau_1,\tau_2)^4+2(\Delta-4)\Delta G_{\uparrow\downarrow}(\tau_1,\tau_2)^2G_{\uparrow\uparrow}(\tau_1,\tau_2)^2\Big].\end{aligned} \tag{3}$$

To the order of $\mathcal{O}(\Delta)$, Eq. (3) can be truncated as

$$\frac{J^2}{2}\Big[G_{\uparrow\uparrow}(\tau_1,\tau_2)^4+G_{\uparrow\downarrow}(\tau_1,\tau_2)^4-4\Delta G_{\uparrow\downarrow}(\tau_1,\tau_2)^2G_{\uparrow\uparrow}(\tau_1,\tau_2)^2\Big]. \tag{4}$$

When $\Delta = 0$, this effective action is identical to the effective action of the Maldacena-Qi model. After considering

the last term in Eq. (4) and rescaling the time variable, the effective action for the reparametrization modes becomes

$$\begin{aligned}\frac{-\mathcal{I}}{N} = \int d\tilde{\tau}\Bigg\{ \left(\left\{ \tanh\frac{t_l(\tilde{\tau})}{2}, \tilde{\tau} \right\} + \left\{ \tanh\frac{t_r(\tilde{\tau})}{2}, \tilde{\tau} \right\} \right) + \tilde{h} \left[\frac{t_l'(\tilde{\tau}) t_r'(\tilde{\tau})}{\cosh^2 \frac{(t_l(\tilde{\tau}) - t_r(\tilde{\tau}))}{2}} \right]^{\mathcal{D}} \Bigg\} \\ + \int \mathrm{d}\tilde{\tau}_1 \, \mathrm{d}\tilde{\tau}_2 \tilde{\Delta} \left[\frac{t_l'(\tilde{\tau}_1) t_r'(\tilde{\tau}_2)}{\cosh^2 \frac{(t_l(\tilde{\tau}_1) - t_r(\tilde{\tau}_2))}{2}} \right]^{2\mathcal{D}} \left[\frac{t_l'(\tilde{\tau}_1) t_l'(\tilde{\tau}_2)}{\sinh^2 \left| \frac{(t_l(\tilde{\tau}_1) - t_l(\tilde{\tau}_2))}{2} \right|} \right]^{2\mathcal{D}}.\end{aligned} \tag{5}$$

where $\tilde{\tau} = \frac{J}{\sqrt{2}\alpha_s}\tau$ is the dimensionless imaginary coordinates time. For the SYK_4 model, $\alpha_s \approx 0.007$ is a positive numerical factor in the action, and the scaling dimension $\mathcal{D} = 1/4$. It's known that the Schwarzian action itself describes the low energy fluctuations of the SYK model, and here we use $\{f, \tau\}$ to denote the Schwarzian derivative. Variable $t_l(\tilde{\tau})$ and $t_r(\tilde{\tau})$ in the low energy action are the time reparametrization modes on the left and right boundaries respectively. We have neglected other modes including the charge fluctuation modes, since they are not excited in our cases. The rescaled coupling constants are

$$\tilde{h} = \frac{h_{\mathrm{tol}}}{4J} \left[\frac{2\alpha_s^2}{\pi} \right]^{1/4}, \qquad \tilde{\Delta} = \frac{\Delta}{8\pi}. \tag{6}$$

These two parameters are related to the magnetic field h_{tol} and the anisotropic paramter Δ. In the equilibrium case, the classical solution assumes the ansatz $t_l(\tilde{\tau}) = t_l(\tilde{\tau}) = t'\tilde{\tau}$, where t' is a constant. The $\tilde{\Delta}$ term could be simplified as:

$$\begin{aligned}(\Delta \text{ term}) &= \int_0^{\tilde{\beta}} \mathrm{d}\tilde{\tau}_1 \int_0^{\tilde{\beta}} \mathrm{d}\tilde{\tau}_2 \tilde{\Delta} \left[\frac{t_l'(\tilde{\tau}_1) t_r'(\tilde{\tau}_2)}{\cosh^2 \frac{(t_l(\tilde{\tau}_1) - t_r(\tilde{\tau}_2))}{2}} \right]^{2\mathcal{D}} \left[\frac{t_l'(\tilde{\tau}_1) t_l'(\tilde{\tau}_2)}{\sinh^2 \left| \frac{(t_l(\tilde{\tau}_1) - t_l(\tilde{\tau}_2))}{2} \right|} \right]^{2\mathcal{D}} \\ &= \int_0^{\tilde{\beta}} \mathrm{d}x_1 \int_{-\tilde{\beta}/2}^{\tilde{\beta}/2} \mathrm{d}x_2 \frac{2t'^2\tilde{\Delta}}{\sinh|t'x_2|} \\ &= \int_0^{\tilde{\beta}} \mathrm{d}x_1 \int_{\Lambda}^{\infty} \mathrm{d}x_2 \frac{4t'^2\tilde{\Delta}}{\sinh(t'x_2)}.\end{aligned} \tag{7}$$

We have employed the ansatz and introduced the new coordinates $x_1 = \frac{1}{2}(\tilde{\tau}_1 + \tilde{\tau}_2)$, $x_2 = (\tilde{\tau}_1 - \tilde{\tau}_2)$. The dimensionless value $\tilde{\beta} = \frac{\beta J}{\sqrt{2}\alpha_s}$. Since the UV divergence of the conformal solution is not physical, we have introduced a natural cutoff $\Lambda = (\epsilon/J)\frac{J}{\sqrt{2}\alpha_s}$, where ϵ is a constant of the order $\mathcal{O}(1)$. Besides, because the effective action describes a zero temperature wormhole, the upper bound of the integration x_2 extends to infinity.

Adding up all the terms, the action reads

$$-\mathcal{I}/\beta = -\frac{Jt'^2}{\sqrt{2}\alpha_s} + \frac{h_{\mathrm{tol}}}{4(2\pi\alpha_s^2)^{1/4}}\sqrt{t'} + \frac{\Delta J t' \log\left(\tanh\left(\frac{t'\epsilon}{2\sqrt{2}\alpha_s}\right)\right)}{2\sqrt{2}\pi\alpha_s}. \tag{8}$$

It is also known that the classical saddle point $\frac{\mathrm{d}\mathcal{I}}{\mathrm{d}t'} = 0$ determines the equilibrium solution as

$$\frac{\mathrm{d}(-\mathcal{I}/\beta)}{\mathrm{d}t'} = -\frac{\sqrt{2}Jt'}{\alpha_s} + \frac{h_{\mathrm{tol}}}{8(2\pi\alpha_s^2)^{1/4}}\frac{1}{\sqrt{t'}} + \frac{\Delta J\left(t'\epsilon\,\mathrm{csch}\left(\frac{t'\epsilon}{\sqrt{2}\alpha_s}\right) + \sqrt{2}\alpha_s \log\left(\tanh\left(\frac{t'\epsilon}{2\sqrt{2}\alpha_s}\right)\right)\right)}{4\pi\alpha_s^2} = 0. \tag{9}$$

After the asymptotic expansion and assuming $t' \ll 1$, we can obtain equilibrium solution as

$$t' = \begin{cases} \frac{1}{4}\left(\frac{\alpha_s h_{\mathrm{tol}}}{J}\right)^{2/3}\left(\frac{1}{8\pi\alpha_s^2}\right)^{1/6} & \Delta = 0, \\ \frac{\Delta}{4\pi}\log\left(\frac{-e\epsilon\Delta}{8\sqrt{2}\pi\alpha_s}\right) + \frac{\Delta}{4\pi}\log\left(-\log\left(\frac{-e\epsilon\Delta}{8\sqrt{2}\pi\alpha_s}\right)\right) + \cdots & h_{\mathrm{tol}} = 0. \end{cases} \tag{10}$$

The $\Delta = 0$ case reproduces the result in Ref. [1]. It is known that, in the gravity interpretation, the energy gap in the TW phase is $E_{\mathrm{gap}} = \frac{J}{\sqrt{2}\alpha_s}t'\mathcal{D}$. Then after using (10), we reveal different contributions of h_{tol} and Δ to the E_{gap} term.

Second, with the value of t', the magnetization M^x can also be calculated by the Green's function:

$$\begin{aligned} M^x &= |G_{\uparrow\downarrow}(t_l(\tau), t_r(\tau))| \\ &= \left(\frac{1}{16\pi J^2}\right)^{1/4} \left[\frac{t_l'(\tau)t_r'(\tau)}{\cosh^2 \frac{(t_l(\tau)-t_r(\tau))}{2}}\right]^{1/4} \\ &= \frac{1}{2(2\pi)^{1/4}} \frac{\sqrt{t'}}{\sqrt{\alpha_s}}. \end{aligned} \tag{11}$$

plugging Eq.(10) into the above relation between M^x and t', the effects of $h_{\rm tol}$ and Δ are shown clearly.

B. Quench Dynamics with Molecular Field Correction

In the subsection A, we have studied the equilibrium properties by the imaginary time approach. In this subsection, we will study the real time evolution of this random spin model, starting from the TW phase. Therefore, we perform the analytically continuation on the action (5) by substituting the coordinate time $\tilde{\tau} \to i\tilde{t} + 0$ ($\tau \to it + 0$) and reparametrization modes $t_{l/r} \to it_{l/r}$. Here, for simplicity, we consider the case with $\Delta = 0$. Subsequently, Eq. (5) becomes

$$\frac{\mathcal{I}}{N} = \int d\tilde{t} \Bigg\{ -\left(\left\{\tan\frac{t_l(\tilde{t})}{2}, \tilde{t}\right\} + \left\{\tan\frac{t_r(\tilde{t})}{2}, \tilde{t}\right\}\right) + \tilde{h}\left[\frac{t_l'(\tilde{t})t_r'(\tilde{t})}{\cos^2\frac{(t_l(\tilde{t})-t_r(\tilde{t}))}{2}}\right]^{\mathcal{D}} \Bigg\}, \tag{12}$$

which is the same as the one in the Maldacena-Qi model. The action has SL(2) gauge symmetry, which means we should require the Noether charge vanishes $Q_0 = 2Ne^{-\varphi}[-e^{2\varphi} - \varphi'' + \tilde{h}\mathcal{D}e^{2\mathcal{D}\varphi}] = 0$ with $t_l'(\tilde{t}) = t_r'(\tilde{t}) = e^{\varphi(\tilde{t})}$[1]. This determines the corresponding quench dynamics, during which the magnetization at coordinate time t can be expressed as

$$\begin{aligned} M^x(t) &= |G_{\uparrow\downarrow}(t_l(t), t_r(t))| \\ &= \left(\frac{1}{16\pi J^2}\right)^{1/4} \left[\frac{t_l'(t)t_r'(t)}{\cos^2 \frac{(t_l(t)-t_r(t))}{2}}\right]^{1/4} \\ &= \frac{1}{2(2\pi)^{1/4}\sqrt{\alpha_s}} e^{\frac{1}{2}\varphi(t)}. \end{aligned} \tag{13}$$

Considering the non-zero $\bar{J}$ effect in the dynamical process, we can substitute $h_{\rm tol}$ as $h_{\rm tol}(t) = -\bar{J}M^x(t)$. Consequently, the equation of motion becomes

$$-e^{2\varphi} - \varphi'' - \frac{\bar{J}}{32\sqrt{\pi}J} e^{\varphi} = 0, \tag{14}$$

with the proper initial conditions for this ordinary differential equation given by

$$\begin{aligned} \varphi(0) &= 2\log\left(2(2\pi)^{1/4}\sqrt{\alpha_s}M^x(0)\right), \\ \varphi'(0) &= 0. \end{aligned} \tag{15}$$

By numerically solving this differential equation, we find that for $\bar{J} < 0$ and $h > 0$, and in a parameter range of $\bar{J}/J$, M^x first decreases and then oscillates around certain non-zero value as time increases.

III. PHASE DIAGRAM

A. Imaginary-Time Approach

Here we introduce more details of two methods that we used to determine the phase diagram. The first one is the imaginary-time approach with which we can directly evaluate the thermodynamical quantities, such as the free

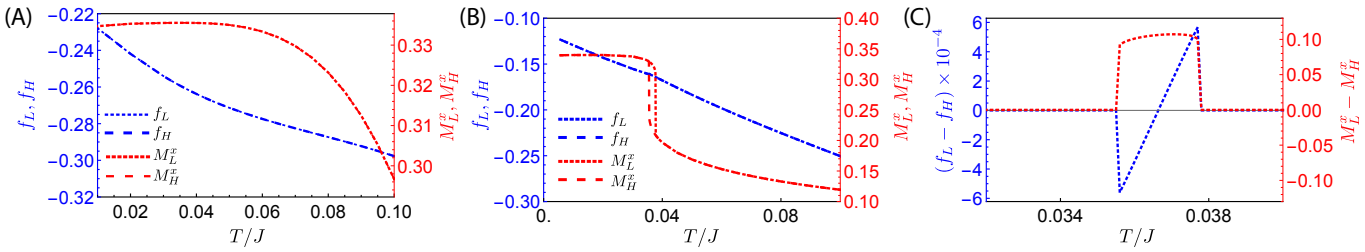

FIG. 2. **Phase Transition Probed by the Imaginary Time Approach.** (A,B) $f_{L/H}$ and $M^x_{L/H}$ denote the free energy and magnetization obtained from the initialization starting from the low-temperature side and the high-temperature side respectively. Here $h_{\rm tol} = 0.2J$, and $\Delta = -0.73$ for (A) and $\Delta = 0$ for (B). (C) The difference between $f_{L/H}$ and between $M^x_{L/H}$ for (B).

energy $f = -\frac{1}{\beta N}\log Z = \frac{1}{\beta N}\mathcal{I}$ (see Eq. (1)) and the magnetization M^x. With the imaginary-time approach, we start the self-consistent calculation from the high-temperature region, initialized with a proper high-temperature initial guess of $G(\tau)$. When the self-consistent solution is reached at a certain temperature, we decrease the temperature and continue the self-consistent calculation for a slightly lower temperature, using the current self-consistent $G(\tau)$ as an initial guess. In this way, we can obtain a series of M^x and f evolving from the high-temperature side, denoted by $M^x_{\rm H}$ and $f_{\rm H}$. The calculation can be carried out similarly by evolving from the low-temperature side, which can also obtain M^x and f denoted by $M^x_{\rm L}$ and $f_{\rm L}$.

After obtaining the thermodynamics data by self-consistent calculation initiated from high- and low-temperature sides, we can determine the two phases and their boundary, as well as the order of phase transitions. For the imaginary time approach, we find both the crossover behavior (Fig. 2(A)) and the first-order transition behavior (Fig. 2(B, C)). At relatively large $|\Delta|$ region $|\Delta| \gtrsim -0.5$, both M^x and f change continuously as lowering the temperature, and solutions initialized from high-temperature or low-temperature are identical. At relatively small $|\Delta|$ region, say $|\Delta| \lesssim 0.5$, thermodynamical properties behave as typical first-order transitions. Both M^x and f show hysteresis effect for two different initializations from high-temperature and low-temperature sides, and a discontinuous jump exists at a certain temperature. Consequently, we can exactly determine the location of the first order transition temperature T^* by the point $f_{\rm H}(T^*) - f_{\rm L}(T^*) = 0$.

B. Real-Time Approach

The second one is the real-time approach. We begin with the greater and lesser Green's functions in real-time defined as

$$\begin{aligned} G^{>}_{ss'}(t_1,t_2) &\equiv -i\frac{1}{N}\sum_l \left\langle c_{l,s}(t_1)c^\dagger_{l,s'}(t_2)\right\rangle, \\ G^{<}_{ss'}(t_1,t_2) &\equiv i\frac{1}{N}\sum_l \left\langle c^\dagger_{l,s'}(t_2)c_{l,s}(t_1)\right\rangle, \end{aligned} \tag{16}$$

as well as the retarded and advanced Green's function defined as

$$G^{R/A}_{ss'}(t_1,t_2) \equiv \mp i\Theta\left(\pm t_{12}\right)\frac{1}{N}\sum_l \left\langle \{c_{l,s}(t_1), c^\dagger_{l,s'}(t_2)\}\right\rangle, \tag{17}$$

where $\Theta(t)$ is the Heaviside step function and we have defined $t_{12} = t_1 - t_2$. $G^{R/A}$ is related to $G^{\gtrless}$ as

$$G^{R/A}(t_1,t_2) = \pm\Theta\left(\pm t_{12}\right)\left(G^{>}(t_1,t_2) - G^{<}(t_1,t_2)\right). \tag{18}$$

In the thermal equilibrium, all Green's functions are only functions of t_{12} due to the time-translational symmetry. To solve the real-time Green's functions self-consistently, we introduce the spectral function as

$$G^R(\omega) = \int {\rm d}z \frac{\rho(z)}{z - \omega - i0}, \tag{19}$$

which implies $\rho(\omega) = -\mathrm{Im}G^R(\omega)/\pi$. Other Green's functions are determined by the fluctuation-dissipation theorem as

$$\begin{aligned} G^<(\omega) &= 2\pi i n_F(\omega)\rho(\omega), \\ G^>(\omega) &= -2\pi i n_F(-\omega)\rho(\omega), \end{aligned} \tag{20}$$

where $n_F(\omega)$ is the Fermi-Dirac distribution function.

To derive the self-consistent equation for the spectral function, we apply the Fourier transformation on the imaginary time self-energy

$$\Sigma(\tau) = -\frac{J^2}{4}\sum_{\alpha\alpha'}\xi^\alpha\xi^{\alpha'}\sigma^{\alpha'}G(\tau)\sigma^\alpha \mathrm{Tr}\left[\sigma^{\alpha'}G(\tau)\sigma^\alpha G(-\tau)\right], \tag{21}$$

with $\Sigma(\tau) \to \Sigma(i\omega_n)$ and perform the analytical continuation $i\omega_n \to \omega + i0$ after the Matsubara frequency summation for the internal dummy frequency [2]. We then obtain $G^R(\omega)^{-1} = \omega + \frac{h}{2}\sigma^x - \Sigma^R(\omega)$, with

$$\begin{aligned} \Sigma^R(\omega) = \frac{J^2}{4}\int_{-\infty}^{\infty} \mathrm{d}t\ \Theta(t)e^{i\omega t} \\ \sum_{\alpha\alpha'}\Bigg(\xi^\alpha\xi^{\alpha'}\sigma^{\alpha'}G^>(t)\sigma^\alpha\ \mathrm{Tr}\left[\sigma^\alpha G^<(-t)\sigma^{\alpha'}G^>(t)\right] - \\ \xi^\alpha\xi^{\alpha'}\sigma^{\alpha'}G^<(t)\sigma^\alpha\ \mathrm{Tr}\left[\sigma^\alpha G^>(-t)\sigma^{\alpha'}G^<(t)\right]\Bigg). \end{aligned} \tag{22}$$

Iteratively solving these equations gives the spectral function $\rho_{ss'}(\omega)(s, s' = \uparrow, \downarrow)$ and real-time Green's functions. Then, we can obtain the spectral ratio we introduced as $r \equiv \rho_{\uparrow\uparrow}(0)/\max_\omega \rho_{\uparrow\uparrow}(\omega)$. By definition, the spectral ratio $r \in [0, 1]$. $r = 0$ means a gap at $\omega = 0$, describing the spectral function of the TW phase as discussed in the main text. $r = 1$ means that the spectral function is peaked at $\omega = 0$, describing the spectral function of the BH phase. Here we can also find different transition types. For the first order transition region, r jumps discontinuously between 0 and 1. And in the crossover region, the gap closes gradually and r changes continuously.

IV. QUENCH DYNAMICS

A. The Kadanoff-Baym Equation.

To study the real-time dynamics, we utilize the Kadanoff-Baym equation on the Keldysh contour [3], which describes the real-time evolution of $G^{\gtrless}$. Assuming the melon diagram approximation and applying the Langreth rules [4] on the Schwinger-Dyson equation, we find that [5]:

$$\begin{aligned} i\partial_{t_1}G^{\gtrless}(t_1, t_2) + \frac{h_{\mathrm{eff}}(t_1)\sigma^x}{2}G^{\gtrless}(t_1, t_2) = \\ \int dt_3(\Sigma^R(t_1, t_3)G^{\gtrless}(t_3, t_2) + \Sigma^{\gtrless}(t_1, t_3)G^A(t_3, t_2)), \\ -i\partial_{t_2}G^{\gtrless}(t_1, t_2) + G^{\gtrless}(t_1, t_2)\frac{h_{\mathrm{eff}}(t_2)\sigma^x}{2} = \\ \int dt_3(G^R(t_1, t_3)\Sigma^{\gtrless}(t_3, t_2) + G^{\gtrless}(t_1, t_3)\Sigma^A(t_3, t_2)). \end{aligned} \tag{23}$$

Here we have taken the contribution of $\bar{J}$ into account by

$$h^x_{\mathrm{eff}}(t) = i\frac{\bar{J}}{2}\left(G^<_{\uparrow\downarrow}(t, t) + G^<_{\downarrow\uparrow}(t, t)\right). \tag{24}$$

The real-time self-energies in Eq. (23) are given by

$$\begin{aligned} \Sigma^{\gtrless}(t_1, t_2) = \frac{J^2}{4}\sum_{\alpha,\alpha'}\xi^\alpha\xi^{\alpha'} \\ \sigma^{\alpha'}G^{\gtrless}(t_1, t_2)\sigma^\alpha \mathrm{tr}\left[\sigma^{\alpha'}G^{\gtrless}(t_1, t_2)\sigma^\alpha G^{\lessgtr}(t_2, t_1)\right], \end{aligned} \tag{25}$$

with $\Sigma^{R/A}$ related to $\Sigma^{\gtrless}$ as

$$\Sigma^{R/A}(t_1,t_2) = \pm\Theta\left(\pm t_{12}\right)\left(\Sigma^{>}(t_1,t_2) - \Sigma^{<}(t_1,t_2)\right). \tag{26}$$

For $t_1, t_2 < 0$, $G^{\gtrless}(t_1,t_2) = G^{\gtrless}(t_{12})$ is given by the equilibrium solution, which serves as the initial conditions for the time dynamics. Evolving $G^{\gtrless}(t_1,t_2)$ using Eq. (23)-(25) gives the quantum dynamics.

To analyze the quench dynamics, we study the spectral function and the quantum distribution function at given time t. We firstly separate the relative time t_r by defining the temporal Green's function $\tilde{G}^{\iota}(t,t_r)$ as

$$\begin{aligned} \tilde{G}^{\iota}(\max\{t_1,t_2\}, t_1 - t_2) &= G^{\iota}(t_1,t_2), \\ \tilde{G}^{\iota}(t,\omega) &= \int dt_r e^{i\omega t_r}\tilde{G}^{\iota}(t,t_r). \end{aligned} \tag{27}$$

Here $\iota \in \{>, <, R, A\}$ and we perform the Fourier transformation for the relative time. The temperal spectral function is then defined as

$$\rho(t,\omega) = -\frac{1}{\pi}\mathrm{Im}\tilde{G}^{R}(t,\omega). \tag{28}$$

Similar as Eq. (27), we could also define $\tilde{\Sigma}^{\iota}$. At thermal-equilibrium, there is no time dependence for both $\tilde{G}$ and $\tilde{\Sigma}$, and the fluctuation-dissipation theorem implies the relation [3]

$$\tanh\frac{\beta\omega}{2} = \frac{\tilde{\Sigma}^{>}(\omega) + \tilde{\Sigma}^{<}(\omega)}{\tilde{\Sigma}^{R}(\omega) - \tilde{\Sigma}^{A}(\omega)}. \tag{29}$$

Then for the non-equilibrium case, motivated by Eq. (29), we define the quantum distribution function at time t as

$$\mathcal{F}(t,\omega) = \frac{\tilde{\Sigma}^{>}(t,\omega) + \tilde{\Sigma}^{<}(t,\omega)}{\tilde{\Sigma}^{R}(t,\omega) - \tilde{\Sigma}^{A}(t,\omega)}. \tag{30}$$

B. Examples

In this section, we provide more examples to support the two main conclusions on the quench dynamics proposed in the main text. Fig. 3 shows the results of the quench dynamics, including the time dependence of the magnetization and the spectral functions in the initial and final states before and after the quench dynamics. In addition, we summarize the examples in the Table. I. Clearly, in all these examples, we can see that

- When initially $r < 1$ and finally $r = 1$, we observe a stretched exponential decay with exponent $\eta < 1$.
- When initially $r < 1$ and finally r is also < 1, we observe that the magnetization saturates at finite value at long time and oscillatory behavior at long time.

[1] J. Maldacena and X.-L. Qi, *Eternal Traversable Wormhole,* arXiv:1804.00491.
[2] J. Maldacena and D. Stanford, *Remarks on the Sachdev-Ye-Kitaev Model,* Phys. Rev. D **94**, 106002 (2016).
[3] A. Kamenev, *Field Theory of Non-Equilibrium Systems* (Cambridge University Press, 2011).
[4] G. Stefanucci and R. Van Leeuwen, *Nonequilibrium Many-Body Theory of Quantum Systems: A Modern Introduction* (Cambridge University Press, 2013).
[5] A. Eberlein, V. Kasper, S. Sachdev, and J. Steinberg, *Quantum Quench of the Sachdev-Ye-Kitaev Model,* Phys. Rev. B **96**, 205123 (2017).

TABLE I. **Summary of the Examples on Quench Dynamics.** Results with various parameters $\bar{J}/J,\ \Delta,\ \beta J$ are summarized in the table. For each given parameter, the results are described with a (decay exponent η/O, initial $\beta J \to$ final βJ, initial $r \to$ final r). Where the symbol O stands for the oscillatory behavior around a non-zero saturation value. Here we recall that spectral ratio $r \in [0, 1]$ and $r \to 0$ means the TW phase and $r \to 1$ means the BH phase.

$\bar{J}/J$	0	
$\Delta \setminus \beta J$	8	12
-0.6	O, $8.0 \to 15.3, 0.28 \to 0.82$	O, $12.0 \to 16.6, 0.00 \to 0.02$
-0.5	0.59, $8.0 \to 12.4, 0.48 \to 1.00$	O, $12.0 \to 18.6, 0.01 \to 0.06$
-0.4	0.86, $8.0 \to 8.2, 0.70 \to 1.00$	O, $12.0 \to 22.5, 0.01 \to 0.51$

$\bar{J}/J$	1	
$\Delta \setminus \beta J$	8	12
-0.6	0.79, $8.0 \to 5.5, 0.28 \to 1.00$	0.49, $12.0 \to 8.4, 0.00 \to 1.00$
-0.5	0.89, $8.0 \to 5.0, 0.48 \to 1.00$	0.75, $12.0 \to 5.3, 0.01 \to 1.00$
-0.4	0.95, $8.0 \to 4.8, 0.70 \to 1.00$	0.91, $12.0 \to 4.3, 0.08 \to 1.00$

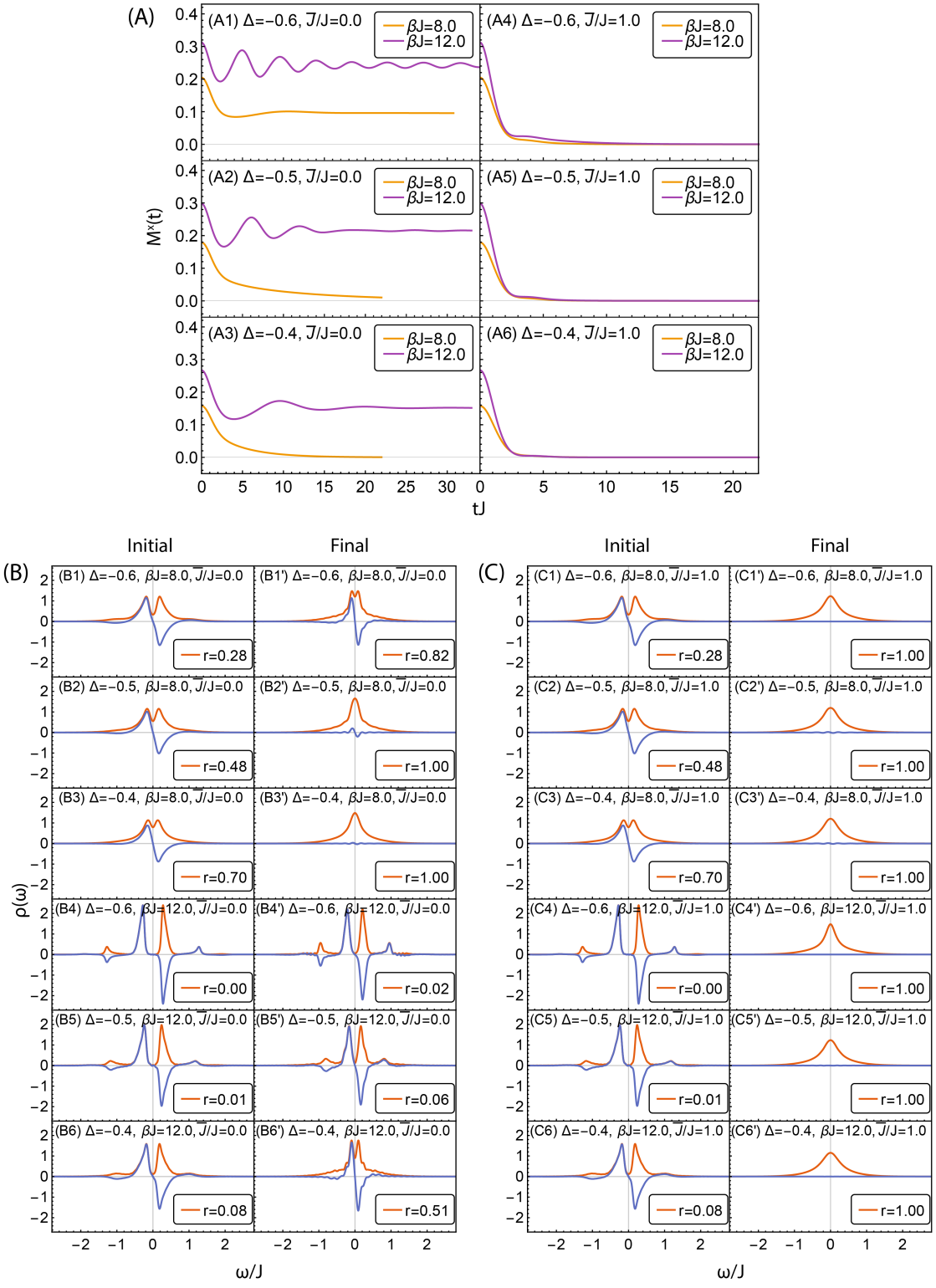

FIG. 3. **More Examples of the Quench Dynamics.** (A) The time dependence of the magnetization for various parameters. (B) Spectral functions for both the initial and the final states with $\bar{J}/J = 0$. (C) Spectral functions for both the initial and the final states with $\bar{J}/J = 1$.